Preliminary Results from an Airborne Experiment Using Along-Track Interferometry for Ground Moving Target Indication

Elaine Chapin, Jet Propulsion Laboratory, California Institute of Technology
Curtis W. Chen, Jet Propulsion Laboratory, California Institute of Technology

Key Words: Synthetic Aperture Radar, Along-Track Interferometry, Ground Moving Target Indication

ABSTRACT

Synthetic aperture radar (SAR) along track interferometry (ATI) has been used extensively to measure ocean surface currents. Given its ability to measure small velocities (~10 cm/s) of relatively radar-dark water surfaces, there is great potential that this technique can be adapted for ground moving target indication (GMTI) applications, particularly as a method for detecting very slow targets with small radar cross sections. In this paper we describe preliminary results from an ATI GMTI experiment.

The SAR data described here were collected by the dual-frequency NASA/JPL airborne radar in its standard dual-baseline ATI mode. The radar system imaged a variety of control targets including a pickup truck, sport utility vehicles, passenger cars, a bicycle, and pedestrians over multiple flight passes. The control targets had horizontal velocities of less than 5 m/s. The cross sections of the targets were not purposely enhanced, although the targets' reflectivities may have been affected by the existence of the GPS equipment used to record the targets' positions. Single-look and multiple-look interferograms processed to the full azimuth resolution were analyzed. In the data processed to date, all of the targets were observed by visual inspection in at least one of the four combinations of dual-frequency, dual-baseline interferometric data. This extremely promising result demonstrates the potential of ATI for GMTI applications.

1. *INTRODUCTION*

Along-track interferometry (ATI) is an interferometric synthetic aperture radar (SAR) technique for mapping the line-of-sight velocities of surface targets [1]. Because velocity-measurement accuracies of a few centimeters per second have been achieved in oceanographic contexts with this technique, ATI holds great promise for ground moving target indication (GMTI). The processing algorithms and performance models used for oceanographic applications do not necessarily apply to the case of detecting moving targets amidst clutter, however. In the oceanographic case, the entire ocean surface acts as a single, large target moving at a nearly uniform velocity, whereas in the GMTI case, the objective is the detection of dim, discrete targets against a stationary background

Unlike the widely-used cross-track interferometric SAR techniques that are able to map surface topography by utilizing data acquired from phase centers separated in the elevation or across-track direction on a moving platform, ATI techniques involve the acquisition of data from phase centers that are separated in the direction of the SAR flight path. SAR images formed from these two phase centers are therefore characterized by a temporal baseline equal to the time required for the platform(s) to travel the distance of the along-track offset (i.e., the physical baseline) between the two phase centers. Thus, while stationary elements of the imaged scene contribute identically to the two images, moving targets in the scene exhibit phase shifts between the two images. An interferogram formed from the two complex SAR images consequently depicts surface movements in the imaged scene, and the system can be made very sensitive to small velocities with the use of a long interferometric baseline.

In addition to their sensitivity to low target velocities, ATI systems can also be made very sensitive to targets with low radar reflectivities. This is because the SAR ATI technique makes use of long coherent integration times that reduce the amount of clutter competing with any given target. An unresolved target of interest competes only with the clutter in a single image pixel, so with appropriate SAR resolution, high signal-to-clutter ratios can be achieved. ATI thus offers the capability of detecting targets too dim to detect by other means. Such long coherent integration times are often not possible with space-time adaptive processing (STAP) techniques in which the coherent processing intervals are limited by sample-support restrictions.

Moreover, ATI techniques are less sensitive to channel mismatch than other GMTI techniques. ATI techniques do not cancel clutter through the complex subtraction of two signals as STAP and displaced phase center antenna (DPCA) techniques do. ATI techniques rely on a conjugate-product operation and involve only two channels, so algorithms for correcting channel bias, topographic effects, etc. are simpler, more efficient computationally, and less demanding of sample support.

While previous ATI experiments relying on oceanographic models have reported anecdotal observations of targets of opportunity or detections of radar-bright targets whose reflectivities were artificially enhanced by retroreflectors [2], little experimental work has addressed the problem of detecting slow, dim, discrete ground targets. To evaluate the suitability of the ATI technique for detecting such objects, we performed a proof-of-concept demonstration utilizing airborne SAR data. In this paper we will describe the experimental setup for the demonstration and the encouraging preliminary analysis and results.

2. EXPERIMENTAL SETUP

The radar data discussed in this paper were acquired opportunistically as "piggy-back" collections during four routine calibration flights of the NASA/JPL AIRSAR system [3,4] on 26 February 2004, 15 April 2004, 17 September 2004, and 6 December 2004. A total of thirteen passes of data were acquired. During each pass, 40 MHz range-bandwidth stripmap SAR data were collected simultaneously at both C-band and L-band from multiple phase centers separated along the fuselage of the NASA DC-8 platform. Figure 1 shows a photograph of the plane and the locations of the C-band and L-band antennas used for along track interferometry. The fully processed SAR image data have a range resolution of 3.75 m and an azimuth resolution of 85 cm. The C-band and L-band along track physical baselines are 1.9 m and 19.8 m, respectively. Typical platform velocities are 200 to 215 m/s, and typical pulse repetition frequencies are 1 kHz. The plane normally flies 8 km above the imaged surface. For twelve of the thirteen passes, the pulse transmissions from the fore antenna were interleaved with the pulse transmission from the aft antenna on a pulse by pulse basis while the pulse echoes were received by both antennas for every pulse. This is done simultaneously for both frequencies. The resulting data allow for full-baseline and half-baseline (as well as zero-baseline) interferometric combinations of the phase centers to be synthesized for both frequency bands.

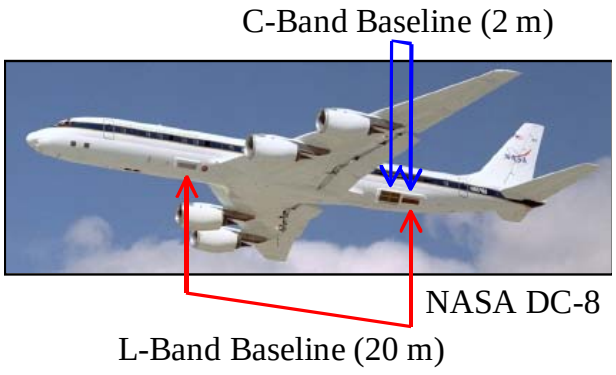

Figure 1: Photograph of the NASA DC-8 showing the positions of the AIRSAR antennas used for ATI.

Figure 2: Photograph of one of the control targets, a Ford F-150 pickup truck, operating during the 17 September 2004 experiment. A GPS antenna is mounted in the bed of the pickup truck.

The collections imaged control targets and targets of opportunity moving amidst a relatively radar-dark scene. The experiment was performed in the Mojave Desert south of the NASA/JPL AIRSAR calibration test site at Rosamond Dry Lake and north of Lancaster, California—a rural area with very little vegetation. Ten of the thirteen of passes view the background scene from the west with very similar imaging geometries. The remaining passes view the same scene from the east with very similar imaging geometries. The passes were repeated and oriented this way to facilitate signal to clutter and signal to noise calculations for the control targets which will be done as follow on work.

A variety of control targets including ordinary passenger cars, sport utility vehicles, a pickup truck, a bicycle, and pedestrians were deployed as control targets. During each pass of radar data, between one and five control targets were imaged. Each control target was equipped with a precision global positioning system (GPS) unit and operated slower than 5 m/s. Figure 2 shows one of the control targets and the character of the scene's terrain and vegetation. Although the cross sections of the control targets were not deliberately enhanced, the GPS equipment used to record the control targets' positions may have increased the targets' backscatter. All of the control targets operated on paved rural roads. The grid of roads at the test site is approximately aligned along track and across track, and some control targets were imaged traveling in both directions.

3. DATA ANALYSIS

We have performed a preliminary analysis of four of the passes of radar data, and the initial analysis is very encouraging. The passes' data were processed using JurassicProk, JPL's advanced interferometric SAR processor for airborne data [5]. We have examined the SAR imagery and both single-look and multiple-look interferograms for both the full and the half interferometric baselines at both frequencies. We have processed data to the full available azimuth resolution at the Doppler centroid of the stationary background, although future work may involve evaluating the impact of different azimuth integration times on target detectability. For the slow velocities of the control targets, however, the Doppler spectra of the targets are expected to match the Doppler spectrum of the stationary background fairly well.

Before attempting to develop a target detection algorithm, we have attempted to answer the more basic question of whether a human observer is able to detect the signatures of the moving targets upon visual inspection of the interferometric data. Consequently, our data analysis thus far has consisted primarily of visual inspection of the single-look and multiple-look interferograms. We have used the GPS data of the control targets' positions and velocities at the imaging times to compute the expected positions of the targets in the interferograms, accounting for the apparent shift of the moving targets in the SAR imagery [6].

The motor vehicle targets moving predominantly perpendicular to the flight direction were easily visible in both the C-band and the L-band interferograms. These targets had radial velocities of 2 to 3 m/s, corresponding to multiple cycles of the interferometric phase for the longer along-track

baselines. The targets appear at the expected positions in the slant plane data products displaced in azimuth from their nominal GPS positions in proportion to their radial velocities.

Figure 3 shows a sample four-look interferogram containing the control target shown in Figure 2 while it was moving roughly perpendicular to the flight direction. The brightness of the image represents magnitude, which is approximately proportional to the amount of signal energy backscattered to the radar. Agricultural fields and roads are visible in the magnitude imagery. The color superimposed on the brightness image represents the interferometric phase. The blue-green color indicates a constant background phase value for the stationary background scatterers in the scene. Objects with suitable line-of-sight velocities appear as different colored dots. The dots should appear shifted in the along track direction (vertically in the images here) relative to the stationary background. The expected shift can be calculated if the range to the target, the velocity of the radar, and the velocity of the target are known [6]. In Figure 3, the purple dot displaced in azimuth above the road near the center of the image in range is the control target.

Figure 4 shows C-band and L-band single-look interferograms for both of the non-zero interferometric baselines that can be synthesized because the antenna used for transmit was alternated. Each interferogram is centered at the expected location of the control target shown in Figures 2 and 3. As with Figure 3, the brightness indicates the magnitude, and the color indicates the interferometric phase. The phase offset of the target is different in each of the four cases because of differences in the effective interferometric baseline. The target appears more smeared in the L-band interferograms than in the C-band interferograms. This is likely due to deviations of the target motion from linear, which cause misfocusing of the target in azimuth, and the longer L-band integration period. The coherent integration times for the C-band and L-band data are approximately 2 s and 8 s.

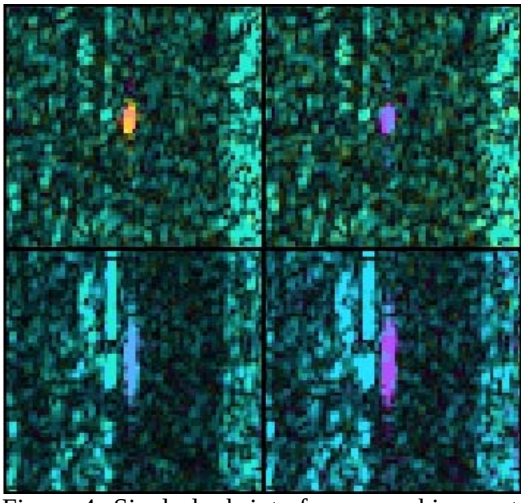

Figure 4: Single look interferogram chips centered on the predicted positions of the control target. The upper two images correspond to the C-Band data while the lower two images correspond to the L-Band data. The left two images correspond to the data with half the effective baseline of the two images on the right. Each chip displays 216.5 m in range and 40.625 m in azimuth. For each chip, range increases across the page while platform flight direction is down the page.

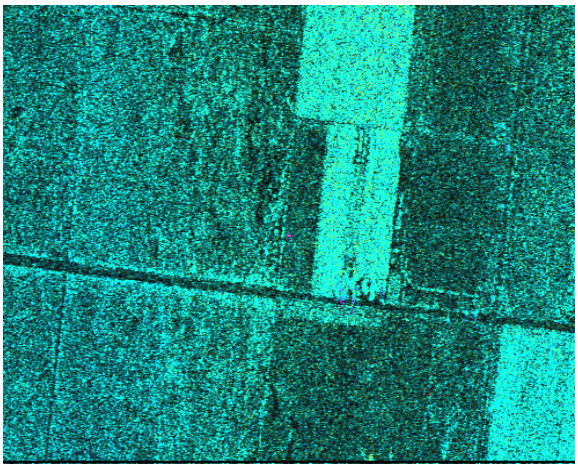

Figure 3: Sample four look C-Band full-baseline along track interferogram showing a control target. Increasing range is to the left of the image. The aircraft's flight direction is down the page. The area represented covers 1630 m in range and 1060 m in azimuth.

The cars and trucks moving predominantly parallel to the flight direction have much lower radial velocities (e.g., 10 cm/s). They were detectable only in the longest baseline L-band interferogram, the interferometric pair with the highest sensitivity to velocity. These targets appear at the expected positions in the slant plane imagery although they are visibly smeared. Such smearing is expected because the along-track component of the target motion gives rise to a mismatch between the target phase history and the reference phase history used for azimuth compression.

Figures 5 and 6 show an example of a control target, in this case a Subaru Legacy station wagon, moving approximately parallel to the flight direction. For this case the radial velocity of the target was 11 cm/s although the horizontal velocity of the target was 2 m/s. The target is visible as the purple dot near the center of the four-look interferogram in Figure 5. Figure 6 shows portions of the single-look interferograms for all four interferometric pairs. The target is not detectable in the C-Band interferograms where the ambiguous velocities are 5.9 m/s and 3.0 m/s, respectively, for the half-baseline and full-baseline interferometric pairs. Because the ambiguous velocities for the L-band cases are 2.4 m/s and 1.2 m/s, the target's phase is more significantly offset from the stationary background making the target visible in the full-baseline L-band data. Comparing Figures 4 and 6, it is clear that the target moving predominantly parallel to the flight track is more smeared than the target moving predominantly perpendicular to the flight track as expected.

In order to examine the limits to which the ATI technique can afford the detection of slow, dim targets; we also deployed a bicycle and pedestrians as control targets. Figure 7 shows a photograph of the bicycle control target. The bicycle was towing a trailer which carried the GPS equipment. Note that parts of the bicycle that were not moving in a nearly linear

fashion (e.g., the wheels and pedals) would not be expected to focus well in the SAR data, so the target signature of Figure 7 is likely due to scattering from the aluminum frames of the bicycle and the trailer, from the GPS equipment, and perhaps from the rider's body. The bicycle had a horizontal velocity of approximately 3 m/s and a radial velocity of 1.5 m/s at the imaging time corresponding to the single look interferograms shown in Figure 8. Because of the target's low reflectivity and the relatively coarse range resolution of the radar data, the bicycle does not have a signal-to-clutter ratio sufficient for it to be visible in the multiple-look interferograms. The bicycle target is visible in the single-look interferograms at both C-band and L-band. (Note that spatial averaging does not enhance the detectability of the target because the target occupies only one resolution cell.) The bicycle target is most clearly visible in the C-band full-baseline interferogram because the bicycle's radial velocity corresponds to an approximately 180˚ phase offset from the stationary background for this baseline. For this baseline, the bicycle appears as a red dot at the center of the image.

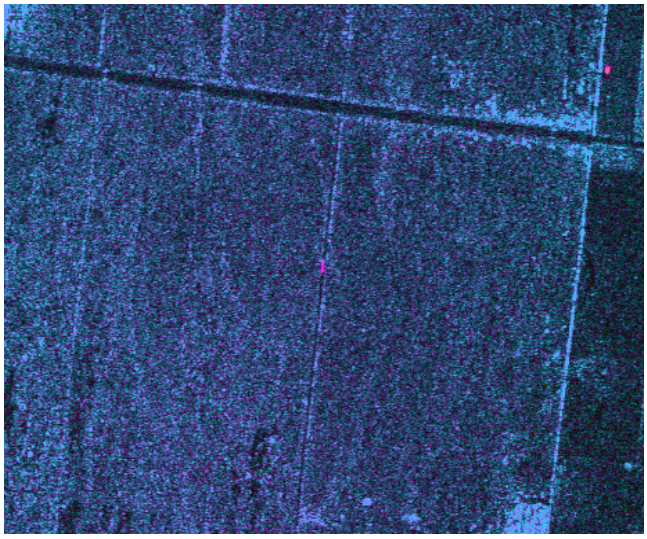

Figure 5: Full-baseline L-Band interferogram centered at position of a target moving predominantly in azimuth. The area imaged covers 1524 m in range and 1025 m in azimuth. The pickup truck shown in Figures 2, 3, and 4 appears as the orange dot in the upper right corner of the image.

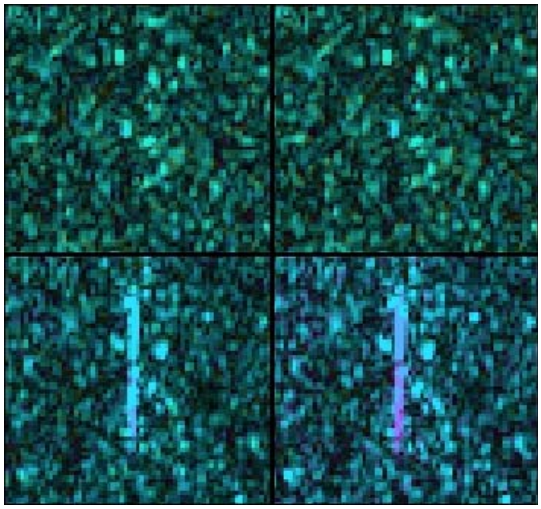

Figure 6: Example of interferograms of a control target moving predominantly in azimuth. The figure is in same format as Figure 4.

Figure 7: Photograph of bicycle control target operating during 15 April 2004 experiment. The target's GPS equipment is mounted on and in the child carrier.

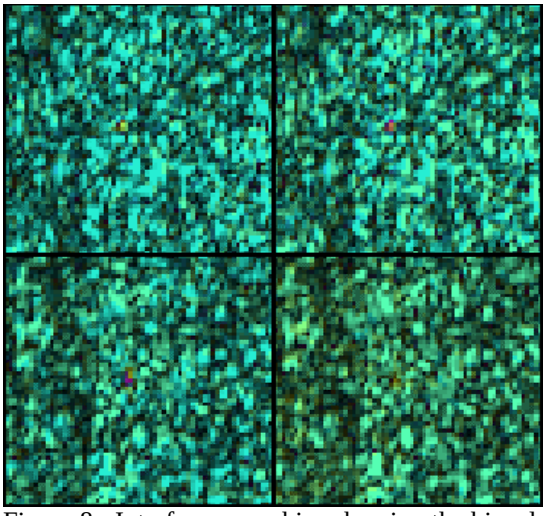

Figure 8: Interferogram chips showing the bicycle. The figure format is the same as Figure 4.

To test the detectability of even slower targets, we also used pedestrians as control targets. Figure 9 shows a photograph of a pedestrian pushing a cart instrumented with high precision GPS equipment. The horizontal velocity of the pedestrian was 1 m/s. The cart consists of a steel frame with upper and lower decks made of wood. The cart may have a strong radar reflection, especially at the L-band wavelength, because of double-bounce phenomena of the VV-polarized signal associated with the vertical members of the cart frame and the flat horizontal surface of the paved road.

Preliminary results for the pedestrian targets are very encouraging. Figure 10 shows the L-band interferograms imaging the pedestrian pushing the electronics cart. Given the low radial velocities, we only expect to see the pedestrian targets in the L-band interferograms since they have smaller ambiguous velocities. Comparing Figures 7 and 9, the pedestrian target is more smeared in azimuth than the bicycle. The smearing may be caused by nonlinear movements of the

Figure 9: Photograph of a pedestrian control target during the 6 December 2004 data collection. The GPS equipment is on the electronics cart.

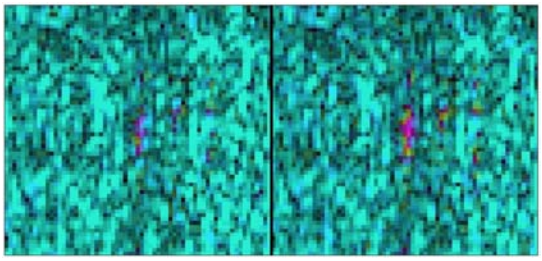

Figure 10: L-Band interferograms imaging the pedestrian pushing the electronics cart. The image on the left corresponds to the interferometric pair with the shorter baseline while the image on the right corresponds to the longer baseline. Each interferogram displays 216.5 m in range and 40.625 m in azimuth. For each chip, range increases across the page while platform flight direction is down the page.

target or by a greater degree of internal motion for the human pushing the cart compared with the bicycle. As expected given its small radial velocity, the target is more easily detected in the full-baseline interferogram.

4. *CONCLUSIONS AND FUTURE WORK*

ATI has potential as a technique to detect ground moving targets with velocities that are too low and cross sections that are too small for other methods. We have conducted an airborne flight test to evaluate this potential. Preliminary analysis of the test data is promising. For this analysis, we formed full resolution interferograms for both available interferometric baselines at both the C-band and L-band frequencies. All of our control targets (cars, sport utility vehicles, a pickup truck, a bicycle, and pedestrians) are detectable upon visual inspection of the interferograms. This result is very encouraging, implying that automated detection may be possible.

The work done thus far is preliminary and does not fully exploit the rich data set or the full capabilities of ATI processing. Only four of the data takes have been evaluated. The processing done on the data thus far has produced the standard oceanographic products. Future algorithmic work includes optimizing the processing to enhance the detection probability and developing detection algorithms. Target and clutter phenomenology will be addressed after the full set of flight lines have been processed and both the control targets and the faster moving targets of opportunity have been evaluated. The processed data will also be used to refine and verify performance models.

Our experiment has revealed the suitability of ATI GMTI for slow, dark targets. This rich data set has given us a peek at what possible future ATI systems, more suitably designed for detecting ground moving targets, may be capable of.

ACKNOWLEDGEMENTS

This work was performed at the Jet Propulsion Laboratory, California Institute of Technology, under a contract with the National Aeronautics and Space Administration. The authors thank Michael Fitzsimmons, Scott Hensley, Michael Jourdan, Charles Le, Thierry Michel, Charles Morris, Ron Muellerschoen, Paul Rosen, Scott Shaffer, and the JPL AIRSAR group for their help in conducting the airborne experiment and processing the data.

REFERENCES

1. R. M. Goldstein, H. A. Zebker, “Interferometric Radar Measurement of Ocean Surface Currents”, *Nature*, vol 328(20), 1987, 707-709.
2. H. Breit, M. Eineder, J. Holzner, H. Runge, R. Bamler, “Traffic Monitoring Using SRTM Along-Track Interferometry”, International Geoscience and Remote Sensing Symposium, vol 2, 2003, 1187-1189.
3. H. A. Zebker, S. N. Madsen, J. M. Martin, K. B. Wheeler, T. Miller, Y. Lou, G. Alberti, S. Vetrella, A. Cucci, “The TOPSAR Interferometric Topographic Mapping Instrument”, *IEEE Transactions on Geoscience and Remote Sensing*, vol 30, 1992, 933-940.
4. D. A. Imel, “AIRSAR Along-Track Interferometry Data”, AIRSAR Earth Science and Applications Workshop, March 2002, http://airsar.jpl.nasa.gov/documents/workshop2002/papers/O1.pdf
5. S. Hensley, E. Chapin, T. R. Michel, “Improved Processing of AIRSAR Data Based on the GeoSAR Processor”, AIRSAR Earth Science and Applications Workshop, March 2002, http://airsar.jpl.nasa.gov/documents/workshop2002/papers/T3.pdf
6. C. W. Chen, “Performance Assessment of Along-Track Interferometry for Detecting Ground Moving Targets”, *Proceedings of the IEEE Radar Conference*, 2004, 99-104.